WWW.ITCMEMS.COM

# Dynamic Analysis of Bifurcating, Non-linear Thin Film Micro-structures

As micro-device application in consumer and commercial products develops, efficient tools are required to simulate device dynamics and assess structural performance. An integrated methodology is developed for studying the dynamics of thin film bifurcating structures
.
Results are presented for a generic thin film structure, which exhibits classical electro-mechanical hysteresis. Such structures can be used to produce light modulating micro-electro-mechanical system (MEMS) devices. Co-authored by Marek Kowarz, Principal MEMS Scientist at ITC.

World-Class
MEMS Innovation

Available online at www.sciencedirect.com
SCIENCE @ DIRECT®
ELSEVIER
Engineering Structures 26 (2004) 1821–1831
ENGINEERING STRUCTURES
www.elsevier.com/locate/engstruct

# Dynamic analysis of bifurcating, non-linear thin film micro-structures

M.W. Carey [a], J. Geoffrey Chase [a,*], A.J. Carr [b], M.W. Kowarz [c]

[a] Department of Mechanical Engineering, University of Canterbury, Private Bag 4800, Christchurch, New Zealand
[b] Department of Civil Engineering, University of Canterbury, Christchurch, New Zealand
[c] Integrated Materials and Microstructures Laboratory, Eastman Kodak Company, 1999 Lake Avenue, Rochester, NY 14650-2015, USA

Received 5 December 2003; received in revised form 1 June 2004; accepted 26 June 2004

**Abstract**

As micro-device application in consumer and commercial products develops, efficient tools are required to simulate device dynamics and assess structural performance. An integrated methodology is developed for studying the dynamics of thin film bifurcating structures. Results are presented for a generic thin film structure, which exhibit classical electro-mechanical hysteresis. Such structures can be used to produce light modulating micro-electro-mechanical system (MEMS) devices.
© 2004 Elsevier Ltd. All rights reserved.

*Keywords:* Dynamic; Finite element; Residual stress; Large deflection; Geometric stiffness; Hybrid stress; Newmark constant average acceleration; Bifurcation; Electrostatic

## 1. Introduction

As the application of capacitively driven micro-electro-mechanical systems (MEMS) in consumer and commercial products develops, efficient tools are required to simulate and characterize the behaviour of such structures [6,7]. Such tools need to provide detailed knowledge of micro- and macro-structural behaviours, a proper understanding of the limitations of the lifetime of such structures and allow the assessment of design and manufacturing variations on structural performance, particularly in high cycle applications.

Fig. 1 shows a generic thin strip micro-structure exaggerated in the vertical direction, in both the unactivated (Fig. 1a) and activated (Fig. 1b) states. The figure illustrates the basic structural element, length $\Lambda$, which can be utilized as a building block in MEMS light modulation applications. The active capacitive electrode is the upper flexible section of the structure and the earth electrode is the lower surface. All intermediate layers are dielectric materials that enhance structural operation while providing electrical isolation. Spacing structures patterned on the lower surface prevent failure due to adhesion during activation.

On application of sufficient voltage, the structure is observed to bifurcate between the two states shown in Fig. 1. When the applied voltage is removed, the structural forces return the device to the unactivated state. It is this binary nature that suits such micro-devices to switching applications. Bifurcation is not the sole domain of thin strip structures. It is also observed in thin cantilever structures, and torsional flaps, used in a variety of sensor and actuator MEMS applications. Examples of MEMS structures under electrostatic actuation include: DMD micromirror device [27], grating light valve (GLV) [3,,13,25], and grating-electro-mechanical system (GEMS) [22–24]. The structure illustrated in Fig. 1 closely resembles the basic ribbon structure of GEMS devices.

Insufficient understanding during design and modelling, results in devices which require large changes in voltage ($\Delta V$) to operate, increasing product costs. Reducing stiffness typically reduces the operating $\Delta V$,

* Corresponding author. Tel.: +64-33642987x7224; fax: +64-33642078.
*E-mail address:* g.chase@mech.canterbury.ac.nz (J.G. Chase).

0141-0296/$ - see front matter © 2004 Elsevier Ltd. All rights reserved.
doi:10.1016/j.engstruct.2004.06.019

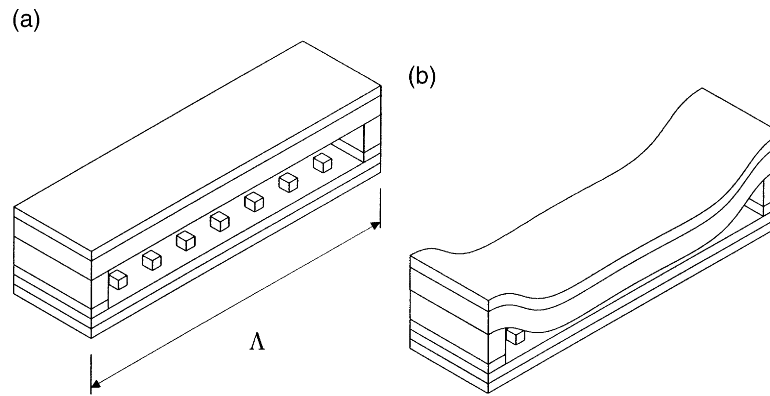


Fig. 1. Capacitive micro-device. (a) Unactivated state; (b) activated state.

but alters performance and can cause undesirable contact between neighbouring structural components. Ideally, non-critical dimensions are minimized reducing stiffness, but care is required to maintain desired structural behaviours.

Accurate characterization of bifurcation and a knowledge of how a device conforms to underlying features is important, particularly in applications where the structure forms part of a reflective array. Thus, sufficient structural information is required to allow an assessment of the precise shape of the reflector formed when the device is active. This shape information is important for understanding aberrations of mirror devices and efficiencies of grating devices. Simulations also allow designers to diagnose problems in manufacturing processes, by establishing acceptable process tolerances on critical parameters and information to assess the effects of variations in structural parameters on device performance, Enabling the production of cost efficient consumer micro-devices.

The dynamics of these MEMS devices are complex involving non-linear position dependent loading, unstable bifurcation, high speed operation, structural contact, anisotropic and variable material properties, large displacements and residual material stresses. Current analysis packages, even those dedicated to modelling micro-devices, do not handle all these phenomena in an integrated fashion. Thus, a general methodology is required that allows the efficient simulation of these phenomena, to enable the optimization of structural performance, while allowing the product designer a through understanding of structural behaviours.

There are three common approaches to modelling thin non-linear structures: reduced order models, string models and finite element models. Reduced order modelling is a popular approach often utilizing a single parameter model of the structural system and a second parameter for the electrostatic system [10,34,37]. Such models, while excellent for global system simulation where the structures' interaction in a larger system is of interest, negate the distributed nature of the structural system severely limiting the structural detail available in simulation results.

Thin structures can be modelled as string structures when membrane tensile forces dominate the structures' stiffness and the structures' mass is low due to small thickness; hence, the structural response is dominated by the membrane force. The cause of such membrane tensile forces is residual material stresses. In MEMS devices, these stresses are due to the dissimilar materials and the fabrication processes used [26,39]. String models include only axial tensile terms ignoring the effects of bending structural contributions. While easy to model using analytical techniques, string idealizations do not allow the modelling of points of zero rotation, making fixed end conditions difficult to capture. String models accurately capture behaviours along the most significant structural dimension but neglect deformation across the structure.

Boundary element models are not commonly used in structural mechanics as the displacement solution is required throughout the structure of interest and not just at the boundaries. However, boundary element techniques are commonly used in the computation of electrostatic forces on arbitrary conductors [29].

Furlani et al. [13] present a method and subsequent results of utilizing an iterative greens function to solve for the static displacement of an electrostatically actuated thin film microbeam, ignoring the dynamics of the system.

A number of specialized software solutions currently exist for solving coupled, electrostatic structural problems. The most common approach couples the publicly available capacitance solver FastCap [29] with a reputable structural solver, using customs software to act as an intermediatory between the external packages. In most published cases, Abaqus is the structural software of choice [14,15,33].

The approach to integrated modelling of electrostatically actuated thin film bifurcating structures can been broken into two sections. First, the physical phenomena required to accurately capture the dynamic behaviours of the structure, expressed for a dynamic finite element model, are outlined. A finite element approach to the dynamic modelling of micro-devices allows simple inclusion of variations in geometry and material properties, as well as a discretization suited to electrostatic analysis. Second, non-linear material and forcing behaviours are implemented within a general, integrated framework.

## 2. Dynamics and solution

The behaviours of thin strip micro-devices are complex involving, momentum and inertia effects, electrostatic loading, residual material stresses, structural contact, and large displacements. All of these phenomena must be considered within an integrated modelling framework.

### 2.1. Dynamics

The dynamics of general structural systems under time varying loading is governed by the second order ordinary differential equation

$$M\ddot{v} + C\dot{v} + Kv = p \tag{1}$$

where $M$, $C$ and $K$ represent the mass, damping and stiffness matrices of the system, respectively, $v$ is a vector representing the deflection of the system, the dot notation denotes derivatives with respect to time, and $p$ is the time varying applied load. Hence, micro-device dynamics are no different to those of larger structures. Dimensions are many orders of magnitude smaller, and the dominance of different effects may vary but the same physical laws apply.

Recognizing the inherent symmetry of the planar model structure allows reduction in the number of degrees of freedom in the numerical model, reducing required solution time at the expense of neglecting contributions from asymmetrical and torsional modes of operation. The dominant loading of the structure is the symmetrical electrostatic load with little influence from fringing field electrostatic interactions with neighbouring structural features.

The system stiffness matrix ($K$) utilizes hybrid stress quadrilateral finite elements [18,19], for both bending ($v_z$, $\theta_x$, $\theta_y$) and membrane ($v_x$, $v_y$, $\theta_z$) contributions. Resulting in a stiffness model with six degrees of freedom per node ($v_x$, $v_y$, $v_z$, $\theta_x$, $\theta_y$, $\theta_z$). Hybrid stress finite elements provide efficient stiffness representations allowing accurate modelling using coarse meshes. The hybrid stress class of finite elements interpolate the stresses ($\sigma$) within the elements using a set of undetermined parameters ($\beta$) as illustrated in Eq. (2):

$$\sigma = P\beta \tag{2}$$

The Adini–Clough–Melosh (ACM) [1,28] or the Bogner–Fox–Schmidt (BFS) [4] finite elements are used for determining a consistent system mass representation for the bending degrees of freedom and membrane geometric contributions to bending stiffness. The ACM and BFS elements are displacement based rectangles. The hybrid stress element formulation is based on stress distributions; the displacement basis allows simple calculation of geometric effects, which is more complex for the stress based hybrids. An isoparametric quadrilateral was used for the inplane membrane mass contributions ($v_x$, $v_y$).

The mixing of element formulations has been shown not to negatively impact accuracy of solutions obtained [16,35]. However, static condensation is utilized to remove the screw rotation ($\theta_z$) when computing the undamped frequencies ($\omega$) and mode shapes ($\hat{v}$), as the resulting mass matrix does not contain contributions in this degree of freedom.

The Newmark [31] family of integration schemes, shown in Eq. (3), are implicit integration schemes that use a total or incremental form of the equation of equilibrium and assume a variation of acceleration during the time step,

$$[M + \gamma\Delta t C + \beta(\Delta t)^2 K]\Delta\ddot{v} = \Delta p - C\{\ddot{v}_n\Delta t\} - K\left\{\ddot{v}_n\frac{(\Delta t)^2}{2} + \dot{v}_n\Delta t\right\} \tag{3}$$

where $M$, $C$, $K$, $v$, $\dot{v}$, $\ddot{v}$ and $p$ are as defined in Eq. (1). $\Delta t$ is the length of the numerical time step, the subscript $n$ indicates the value at the start of the time step. $\gamma$ and $\beta$ are parameters defining the acceleration assumption during the time step. The two most common schemes are the linear ($\gamma = 1/2, \beta = 1/6$) and constant average acceleration ($\gamma = 1/2, \beta = 1/4$), the latter was used due to its unconditionally stable behaviour. The Newmark constant average acceleration (NCAA) is unconditionally stable but not unconditionally accurate. As $\Delta t$ is reduced, the error in the resulting acceleration decreases.

The incremental form of the NCAA is defined [8,20]:

$$\left(\frac{4}{\Delta t^2}M + \frac{2}{\Delta t}C + K\right)\Delta v = p_{n+1} + M\left(\frac{4}{\Delta t}\dot{v}_n + \ddot{v}_n\right) + C\dot{v}_n - Kv_n \tag{4}$$

$$\Delta\dot{v} = \frac{2\Delta v}{\Delta t} - 2\dot{v}_n \tag{5}$$

$$\Delta\ddot{v} = \frac{4\Delta v}{(\Delta t)^2} - \frac{4\dot{v}_n}{\Delta t} - 2\ddot{v}_n \tag{6}$$

These equations compute the changes in displacement ($\Delta v$), velocity ($\Delta \dot{v}$) and acceleration ($\Delta \ddot{v}$) from the structural state at the start of the time step ($v_n$, $\dot{v}_n$, $\ddot{v}_n$) from the forces at the end of the time step ($p_{n+1}$).

### 2.2. Large deflection

The deformation of such micro-device structures can be characterized as small, with deflections typically on the order of nanometer and structural dimensions in the micrometer range. However, as the structure deforms, the initial planar system model must be updated to include the effects of the deformation. They are Commonly termed large deflection effects, as the structural configuration is significantly different from the original configurations.

For thin film structures, two criteria need to be considered, the strain in the structure and the local rotation experienced. The technique for updating the system configuration to reflect these changes utilizes transformations to map the local system properties to the global orientation. This transformation involves rotating the frame of reference and the source of the material non-linearity in the structure. A treatment of such effects is covered in Ref. [36].

For the structure of interest modelling indicated, the inclusion of large deflection effects only gave rise to a 1% change in the observed deflection characteristics. Thus, due to the increased computational overhead of the additional assembly steps required, large deflection effects were implemented within the model framework; however, they were not enabled during the gathering of the results presented.

### 2.3. Residual material stresses

Often considered a second order effect in the structures where initial material stresses are small and subsequently neglected, the contribution of inplane initial material stresses [39] on micro-device performance must be considered, as it acts to laterally stiffen the structure [32,38]. As the characteristic dimensions of such structures are small, the resulting inherent stiffness is also small, In the presence of residual stress, which can be many orders of magnitude greater than the inherent stiffness. For example, $Si_3N_4$ where the residual stress can be in excess of 1 GPa [26], these second order effects become significant and can dominate the resulting structural response. Inclusion of the initial material stresses requires two additions to the model: the initial membrane tensile forces, to correctly model the forces in the structure, and the additional bending stiffness.

Initial stress effects are not included in the standard hybrid element formulation; however, it is straight forward to include such effects by redefining the hybrid stress functional to account for the non-zero initial state, as shown in Eq. (7),

$$\sigma = P\beta + P_F\beta_F \quad (7)$$

where $\sigma$ is the stress within the element, $P$ is the stress interpolation and $\beta$ is the coefficients that define the stress state within the element. The quantities with subscript $F$ extend the standard definition for $\sigma$ to include the initial stress conditions. Completing the derivation results in an additional term ($E$) in the hybrid stress functional, Eq. (8).

$$\sum_n(-G^T H^{-1} G v + G^T H^{-1} E + \bar{Q}_T) = 0 \quad (8)$$

where $G$ and $H$ are standard hybrid stress functional terms [18,19], $v$ are the nodal deflections and $\bar{Q}_T$ is the consistent nodal load vector. $E$ is calculated using existing information from the standard hybrid stress formulation ($G$ and $H$), and represents the equivalent nodal forces resulting from the residual stress, in the material, and is added to the applied nodal loads before time history integration is performed.

The additional stiffness introduced by residual stress is identical to increasing the tension on a wire line. As the tensile force increases, additional lateral force is required to achieve a specified lateral deflection. It is not possible to compute the additional stiffness contributions using a hybrid stress element formulation. Either the ACM [1,28] or BFS [4] displacement finite element formulations can be used giving very similar results. The contributions to system stiffness from the residual stress can be calculated for each element and assembled using existing techniques. A constant thickness ACM element has been used with additional stiffness contribution calculated using Eq. (9), where $w$, the standard ACM interpolation polynomial, and $A$, the ACM interpolation matrix, are defined in Ref. [38] and $t$ is the element thickness. The additional stiffness $K_g$ is included in the equilibrium equation, Eq. (1), for use in the dynamic simulation of micro-devices, Eq. (10).

$$K_g = t\int\int A^{-1^{\mathrm{T}}}\left\{\frac{\mathrm{d}w}{\mathrm{d}x}\ \frac{\mathrm{d}w}{\mathrm{d}y}\right\}\begin{bmatrix}\sigma_{xx} & \tau_{xy}\\ \tau_{yx} & \sigma_{yy}\end{bmatrix}\left\{\begin{matrix}\frac{\mathrm{d}w}{\mathrm{d}x}\\ \frac{\mathrm{d}w}{\mathrm{d}y}\end{matrix}\right\}A^{-1}\,\mathrm{d}y\mathrm{d}x \quad (9)$$

$$M\ddot{v} + C\dot{v} + (K + K_g)v = p \quad (10)$$

### 2.4. Electrostatic loading

Electrostatic loading is non-linearly position dependant, as it is generated by the electric field between the two charged surfaces. The applied potential difference across a conductor pair causes the conductors to experience attraction. Modelling forces on capacitive

elements requires the computation of the electric field surrounding the capacitive elements, including the effects of any dielectric materials that may be present, and subsequently determining the forces on the conductors due to the presence of the electric field.

Computation of electrostatic forces is typically performed using boundary element formulation in a package such as FastCap [29]. However, this tool requires that the model state be expressed in a separate file format. Adopting a finite element approach to the solution in the electrostatic domain is also difficult as it requires remeshing or mesh adaption for each update to the structural configuration, which is computationally expensive. Furlani et al. [13] has shown that for simple planar structures utilizing a parallel plate capacitor model is sufficient, particularly when the movable conductor is the active electrode and the substrate acts as earth.

The existing finite element discretization is utilized as the basis for computing the forces on the movable structural elements. The element discretization describes a series of small parallel plate capacitors which, as the mesh is refined, provide an increasingly accurate approximation of the electrostatic forces on the movable electrode.

The formulation for the specific parallel place capacitor model ignores the contributions from the small spacing structures between the conductors as 2D finite element modelling has shown that they only act as local concentrators of electric field and have little effect on the total force experienced by the conductors.

The governing force relationship for the parallel plate capacitor shown in Fig. 2 can be obtained by using the Maxwell stress tensor [11] or virtual work approach,

$$p_z = \frac{-\varepsilon_D \varepsilon_0 V^2 wl}{2[\varepsilon_0 t_D + \varepsilon_D (t_A - v_z)]^2} \tag{11}$$

where $\varepsilon_0$ and $\varepsilon_D$ are the dielectric permitivities of free space and the structural ribbon material, respectively, as illustrated in Fig. 2. Eq. (11) states that the force generated between conductors is proportional to the inverse of the square of the movable electrode deflection. Thus, as the structure deforms the force increases, requiring an iterative approach to determining the structural equilibrium state at the end of each time step.

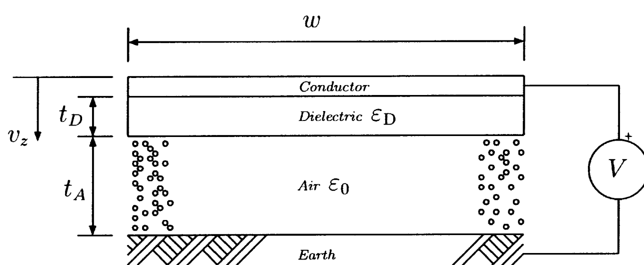


Fig. 2. Parallel plate capacitor definition.

An iterative approach to the structural solution is also required as the NCAA method requires the forces on the structure at the end of the time step ($p_{n+1}$) in order to determine the structural state at the end from the state at the beginning of the time step ($v_n$, $\dot{v}_n$, $\ddot{v}_n$). Iteration is required to determine the correct set of structural displacements and electro-static forces during each numerical time step, this iteration is called self-consistent-electro-mechanics (SCEM) [33]. The relaxation algorithm is typically used to determine when electrostatic equilibrium has been achieved but more efficient methods also exist [5].

For simple micro-device structures, the relaxation algorithm has been shown to be sufficient, as the additional solution complexity, of the other methods, is not warranted. Integrating such a procedure with the NCAA is not currently well documented. However, if more complex device geometry is utilized and alternative dynamic procedures considered, equilibrium can be achieved more efficiently [5].

## 2.5. Bifurcation

Bifurcating thin strip structures exhibit two inherently stable states shown schematically in Fig. 3, and switch in a binary fashion between these two states on the application of sufficient voltage. These two states are the key feature of bifurcating structures that suits them to switching applications. Fig. 3a is the natural state of the structure with no load applied ($V = 0$). To change state, a voltage greater than the pull down voltage ($V_{PD}$) is required. The force on the structure increases as an inverse quadratic function of gap between the structure and ground electrode, Eq. (11). Thus, a point exists where the applied force exceeds the restoring ability of the structure.

This effect can be shown mathematically by examining Eq. (1) and recognizing that the applied load ($p$) is proportional to the inverse of the square of displacement,

$$p \propto \frac{1}{v^2} \tag{12}$$

Thus, Eq. (1) reduces to,

$$M\ddot{v} + C\dot{v} + \left(K - \frac{\chi}{v^3}\right)v = 0 \tag{13}$$

where $\chi$ is a proportionality constant. Thus, for a given velocity and acceleration, a voltage and displacement exist such that the system exhibits zero stiffness. Assuming that small deflection theory applies and $K$ does not change, Eq. (13) resembles a constrained

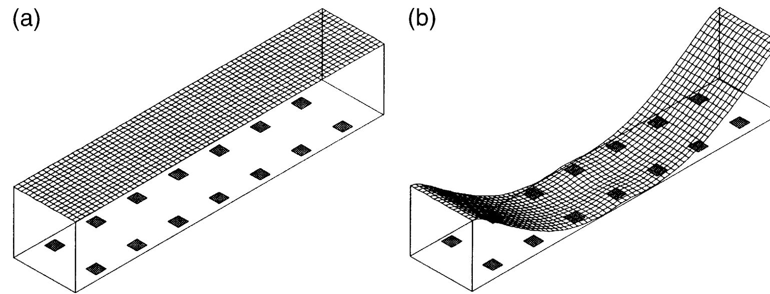


Fig. 3. Finite element mesh of stable structural states. (a) Unactivated state ($V = 0$); (b) activated state ($V > V_{PD}$).

buckling problem. At this point, additional voltage only acts to accelerate the structure and for little change in applied voltage large changes in displacement are realized as the structure bifurcates to the new stable position. The voltage at this bifurcation point is commonly termed the pull down voltage ($V_{PD}$). Deflection is limited by spacing structures on the low surface, as shown in Fig. 1 and again as shaded regions in Fig. 3.

When contact with the underlying structural elements occurs, the displacement of the contacted portions of the movable structure stops as additional constraint is enforced, changing the behaviour of the system. Additional applied forces are distributed in the new system causing deflection where the structure is least stiff, in the non-contacted regions. This phase of operation is termed zipping and occurs in an extremely short period of time. Zipping ends when the structures' ability to resist additional force balances that of the additional applied load. Thus, the second stable state is reached, as shown in Fig. 3b.

Increasing the voltage above this value typically yields little change in displaced shape, with extreme voltages required to pull the remaining free portions of the structure into contact with the standoffs or underlying substrate. Decreasing the applied voltage reduces the number of points of contact and release ensues, starting with the outer most contact points moving back toward the point of first contact. Eventually, the stiffness of the system becomes positive once more, at the release voltage ($V_{RL}$) and the structure resorts to the initial stable state. Structural conditions stipulate that $V_{RL} < V_{PD}$ thus electro-mechanical hysteresis is observed as a result of bifurcation.

### 2.6. Contact

The principal concerns when modelling contact between structural elements are:

1. No energy be added to or removed from the dynamic structural model, to preserve bouncing phenomena,
2. The structure be allowed to break contact freely, and not be artificially constrained, allowing an accurate determination of the release, and voltage ($V_{RL}$),
3. Accurately capturing the time of contact, this is important as it allows accurate calculation of the pull down voltage ($V_{PD}$).

Common approaches to the modelling of contact use penalty functions, which apply psuedo-loads to structural nodes to enforce penetration constraints [17]. Other methods introduce the stiffness and mass of the contacted structure into the dynamic model.

Determining when a model node should experience additional constraint is critical to accurate determination of $V_{PD}$ and $V_{RL}$. Thus, it is important that at each numerical integration step, all additional constraints arising due to contact be removed from the model and the model be allowed to freely deform. If during this initial step model nodes make contact, additional constraint is applied and the step repeated to determine the effects of the additional constraint.

Adding additional constraint to the model can be achieved using three approaches:

1. Clear rows and columns of system matrices ($K$, $M$ and $C$) and apply a psuedo-load equal to the desired displacement, at the degree of freedom (DOF) in contact. This method disconnects contacted portions from the surrounding structure, resulting in a loss of connectivity and stiffness, unacceptably altering system dynamics, and removing draping behaviour from simulation results.
2. Add structural mass and stiffness to contacted DOF representing the underlying structure. Such an approach does not give an exact surface with which contact occurs as the velocity and acceleration of the incoming structure varies. Difficult to distribute mass and stiffness associated with the additional structure accurately. It is not sufficient to include only intermediate structural elements, as these may be smaller than the structure of interest, thus reflecting energy from the immovable boundary.

3. Recognizing that it is possible to augment Eq. (4) as the changes in displacement for the contacted nodes are known a priori, retaining system connectivity and preserving draping behaviours.

Accurately modelling contact between movable and stationary structural components, requires consideration of the energy transferred between the participants. In the case of micro-devices which are often assembled to form part of a product that is many orders of magnitude larger, with much larger mass and stiffness, than that of the movable structural element, consideration must include the extent of the model. In this research, the micro-device is the structure of interest not the system as a whole.

During such a collision, energy is transferred from the structural components in motion to the stationary components. How much energy is transferred is important as this determines if the movable components bounce or adhere after collision.

Using a discrete approach to integration in the time domain often causes large acceleration impulses as a structure comes to rest. These impulses can then propagate further into the model, causing the structure to bounce. Limiting the effects of the acceleration impulse by scaling the magnitude is a possible approach to mitigating the negative effects of a collision between a movable and perfectly fixed rigid structure. Determining the exact scaling required, requires experimental data for a specific structure. In the absence of such data, truncating the impulse is the only alternative.

The dynamic time step size ($\Delta t$) must be controlled to determine when contact between the structure of interest and the surrounding structure first occurs. This control is achieved by allowing a small penetration buffer in the surrounding structural elements, which is insignificant compared to the actual characteristic dimensions.

$\Delta t$ is reduced as new structural nodes penetrate the surrounding structure until the penetration is acceptable and the node is deemed to be in contact. For dynamic modelling using the NCAA, it is difficult to know when to grow $\Delta t$, to maintain computational efficiency. This issue is overcome by attempting to constantly grow the $\Delta t$ back to an efficient base value.

### 2.7. Fluid damping

In structural mechanics, the specific mechanism causing structural damping is often unknown. However, for structures with small characteristic lengths, the mechanism is easily identified as pressure loading due to movement through air [21,30]. For complex structures involving interactions from adjacent elements, determining damping effects is inherently complex requiring a solution to the Navier Stokes equation. Some thin film structures pump fluid between the movable and stationary elements, causing non-uniform pressure gradients in arrayed configurations. For all its added complexity, fluid damping is commonly simplified by modelling the fluidic effects as a lumped parameter system [12,40]. Unless fluid damping can be shown to have significant impact on the dynamics of the structure of interest, commonly accepted equivalent viscous damping methods can be used. Rayleigh damping is widely used in the field of structural analysis. Rayleigh damping is a member of the Caughey [9] family of damping models.

Comparisons between Eastman Kodak experimental data [23] and the fundamental undamped natural frequency of the numerical model indicated that in the regions of interest damping did not significantly impact the numerical results obtained. Thus, a Rayleigh damping model was adopted with 5% critical damping in modes 1 and 10.

### 2.8. Solution

Integrating residual stress, electrostatic loading, contact, large deflections into a dynamic finite element framework utilizing the NCAA scheme to perform numerical integration, results in the basic decision structure shown in Fig. 4.

Each rectangular block in Fig. 4 represents a modular block of simulation code responsible for computing global effects from elemental contributions. The *assembly* module performs the assembly of the contribution to global system matrices ($M$, $K$, $C$) from the elemental contributions. The *forces* module calculates the global forces on the structure from the elemental parallel plate results.

The oval blocks in Fig. 4 represent a computational operation on the system model. *NCAA* captures the dynamics of the system using the NCAA scheme. *Contact* models the effects of structural contact and internally reuses the *NCAA* module.

The diamonds in Fig. 4 represents the controlling logic of the solution procedure and the corresponding branches in the solution path. Implementing the solution in a cohesive environment allows control of the solution from a single language, without the need to translate formats during each solution step. A framework based approach allows inclusion of additional effects at points in the future utilizing the known behaviours of the existing code base.

The outer loop in Fig. 4 controls the time step size, the number of time steps in a block and the writing of results to permanent storage. The inner loop enforces electrostatic equilibrium in each numerical time step. And the miscellaneous branches control the contact and large deflection phenomena.

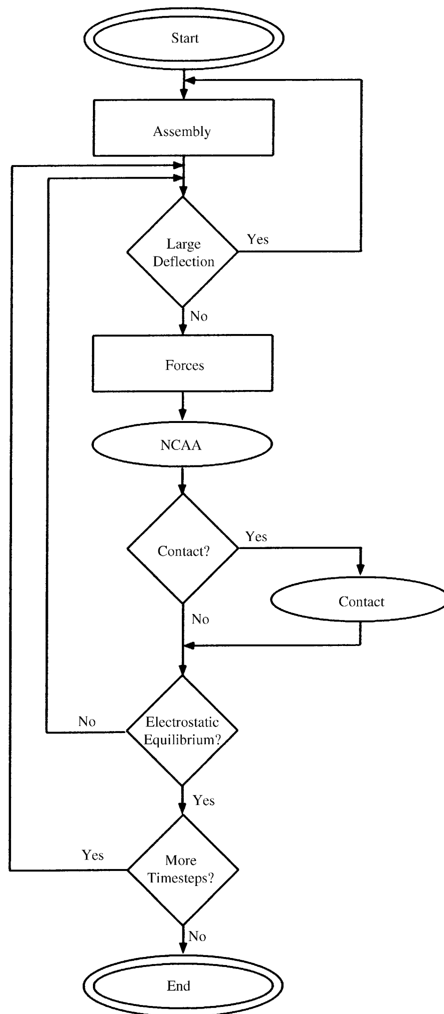


Fig. 4. Implementation framework.

## 3. Simulation and results

Utilizing the methodology and framework developed, a sample analysis is performed on a thin film bifurcating strip structure and the results compared with existing string models. Eastman Kodak string models for the GEMS device were used as the basis for comparison [23]. The model structure consists of a single layer thin film micro-device suspended above a regular array of spacing structures, shown shaded in Fig. 5. The structure is fixed ($v_z = 0$, $\theta_y = 0$) along the $x = 0$ and $x = 30$ edges. The critical dimensions for the model device are listed in Table 1.

Using this structure, the natural frequencies and dynamic mode shapes were determined, providing a value for the initial time step size ($\Delta t$) in the Newmark integration scheme. The full dynamic model is then subjected to a ramped increase in voltage followed by a ramped decrease in voltage. The results exhibit the hysteresis arising from the bifurcating behaviour and device profiles comparable to existing thin film models.

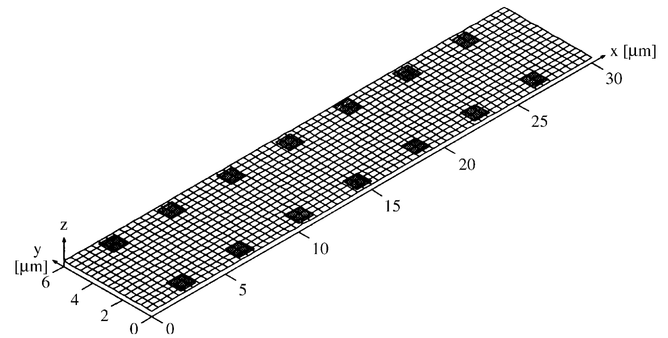


Fig. 5. Model structure.

The modal frequencies of the structure are listed in Table 2 and the first eight mode shapes are illustrated in Fig. 6. For the purposes of comparison, the frequencies and mode shapes of the model structure with residual stress, $\sigma_0 = 0$, are also listed in Table 2. The $\sigma_0 = 0$ case are listed with the corresponding mode shape. The dominance of the residual stress on the performance of the model structure is clearly evident, not only in the dramatic increase in the fundamental frequency, but also in the modification of the order in which modes are excited. The results verify the basic stiffness and mass matrices as well as the system assembly procedures, as the results obtained are within ±2% of the ANSYS results.

A unique feature of specific thin film bifurcating devices is the electro-mechanical hysteresis exhibited

Table 1
Model structure parameters

| Parameter | Value | Units |
|---|---|---|
| Length ($l$) | 30 | µm |
| Width ($w$) | 6 | µm |
| Thickness ($t$) | 0.13 | µm |
| $E$ | 250 | GPa |
| $\nu$ | 0.33 | |
| $\rho$ | 3484 | kg m$^{-3}$ |
| $\sigma_0$ | 850 | MPa |

Table 2
Model structure and ANSYS natural frequencies

| Mode shape | Model structure (Table 1) (MHz) | ANSYS (MHz) | Model structure ($\sigma_0$= 0) (MHz) |
|---|---|---|---|
| 1 | 8.64 | 8.64 | 1.29 |
| 2 | 9.39 | 9.46 | 4.22 |
| 3 | 17.41 | 17.44 | 3.56 |
| 4 | 19.03 | 18.93 | 8.72 |
| 5 | 26.42 | 26.53 | 6.99 |
| 6 | 28.83 | 28.76 | 13.76 |
| 7 | 35.42 | 36.03 | 34.41 |
| 8 | 35.79 | 36.10 | 11.59 |
| 9 | 38.98 | 39.03 | 19.52 |
| 10 | 41.07 | 41.43 | 37.49 |

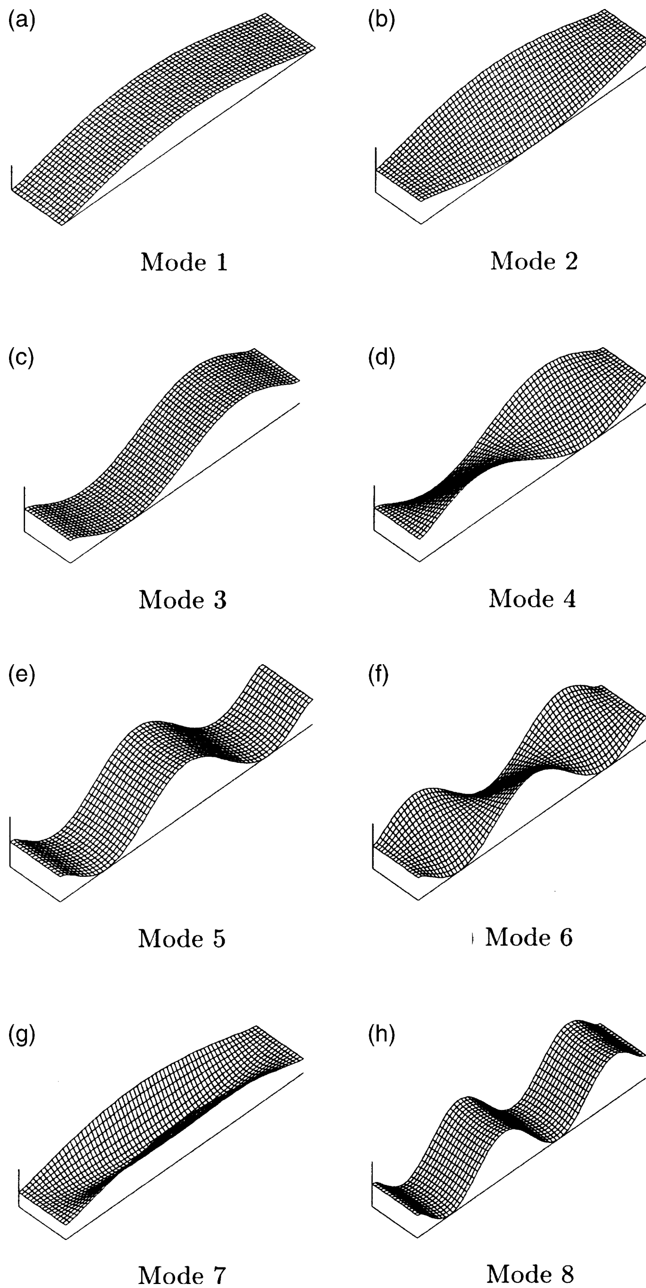


Fig. 6. Model structure undamped dynamic mode shapes 1–8.

during device operation. Fig. 7 displays the hysteretic load–deflection behaviour of the center point of the model structure ($x = 15$ μm, $y = 3$ μm), when a full dynamic simulation of the model structure is performed in the presence of a ramp voltage increase ($0 \rightarrow 25$ V) followed by a ramped voltage decrease ($25 \rightarrow 0$ V) in a total of 50 μs. The bulk structural material is modelled as silicon nitride ($\varepsilon_D = 66.4 \times 10^{-12}$(F/m)) and the surrounding medium air ($\varepsilon_0 = 8.85 \times 10^{-12}$(F/m)) [2]. Fig. 7 clearly shows the pull down and release voltages for the model structure, as well as the ringing observed on device release. The lack

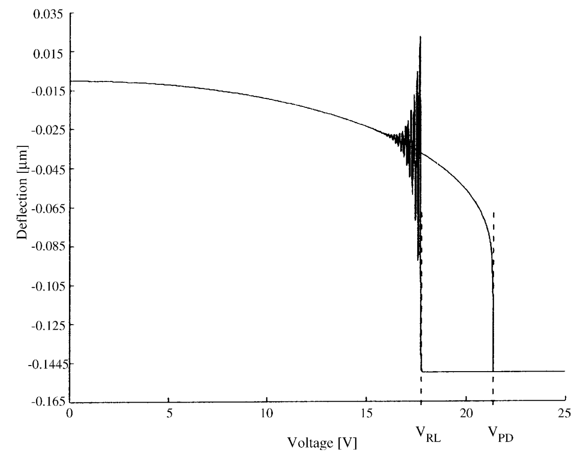


Fig. 7. Electro-mechanical hysteresis.

of bounce when initial contact is made is the result of the truncation of the acceleration impulse.

Comparing the centerline profile ($y = 3$) of the dynamic model structure, with the profile of a string approximation of the same structure, reinforces the efficiency and effectiveness of using string based models in determining the cross-sectional profile. Fig. 8 displays the finite element profile, shown with a solid line, with the string profile, a dashed line. Note that contact constraints for the string model were a solid surface, where as the finite element model utilized a regular array of supports, shown shaded in Fig. 5.

Fig. 8 illustrates the inability of the string model to capture points of zero rotation. The figure also shows that the string model utilizes a plane of symmetry, but because continuity of rotations cannot be enforced the structure appears discontinuous at the plane of symmetry.

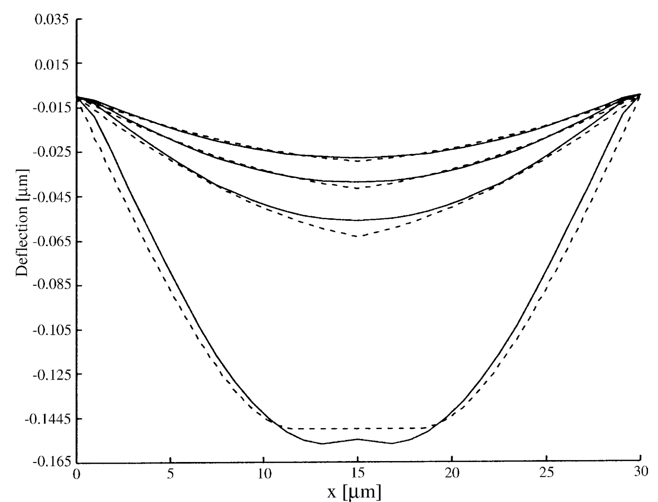


Fig. 8. Profile comparisons.

The figure also captures the thin strip sagging below the level of the underlying structural components, as a result of the additional contact between the strip and the array of supports.

## 4. Conclusions

Implementing residual stress, electrostatic loading, contact, large deflections into a dynamic finite element framework utilizing the NCAA scheme to perform numerical integration provides a platform to study the dynamics of distributed structural deformation for thin film micro-devices. The integrated approach to solution allows an accurate understanding of structural motion, including both velocity and accelerations, a proper knowledge of structural behaviours at critical locations within the structure, provides vital information for understanding the service requirements of very high cycle devices, and allows the device designer a cost efficient method for assessing the impact of fabrication and design variations on device operation.

The illustrated example demonstrates the dominance of residual stress effects on structural dynamics, the conformal behaviour of the structure and the effect this has on the structures suitability as a member of a light modulator array, the bifurcating behaviour including the observed electro-mechanical hysteresis and oscillation on release. Accurately capturing these dynamic effects allow the engineering of more reliable micro-devices for tomorrows' products.

## Acknowledgements

The authors wish to acknowledge the financial and technical support of the Eastman Kodak Company.

## References

[1] Adini A, Clough RW. Analysis of plate bending by the finite element method. NSF report for grant G-7337; 1960.
[2] Bauccio M. ASM Engineered Materials Reference Book, 2nd ed. ASM International; 1994.
[3] Bloom DM, Sandejas FSA, Solgaard O. Method and apparatus for modulating a light beam. US Patent 5,311,360; 1994.
[4] Bogner FK, Fox RL, Schmidt LAJ. The generation of inter-element compatible stiffness and mass matrices by the use of interpolation formulas. Proc. Conf. Matrix Methods in Structural Mechanics. 1965.
[5] Cai X, Yie H, Osterberg P, Gilbert J, Senturia S, White J. A relaxation/multipole-accelerated scheme for self-consistent electromechanical analysis of complex 3-D microelectromechanical Structures, Proc 1993 IEEE ACM Int Conf Comput Aided Design. 1993, p. 283–6.
[6] Carey MW. Dynamic analysis of an optical MEMS device. Masters Thesis, University of Canterbury, Department of Mechanical Engineering, Christchurch, New Zealand. 2003.
[7] Carey MW, Chase JG, Carr AJ, Kowarz MW. Bifurcation dynamics of conformal non-linear thin film micromechanical structures. Proceedings of the 10th Asia-Pacific Vibration Conference (APVC 2003), Gold Coast, Australia, November 12–14, 2003, vol. 1. 2003, p. 31–6.
[8] Carr AJ. RUAUMOKO, the Maori God of volcanoes and earthquakes. Department of Civil Engineering, University of Canterbury; 2001.
[9] Caughey TK. Classical normal modes in damped linear systems. Journal of Applied Mechanics 1960;27:269–71.
[10] Chen J, Kang SM. An algorithm for automatic model-order reduction of nonlinear MEMS devices. IEEE International Symposium on Circuits and Systems 2000.
[11] Davey K, Klimpke B. Computing forces on conductors in the presence of dielectric materials. IEEE Transactions on Education 2002;45(1):95–7.
[12] Furlani EP. Theory and simulation of viscous damped reflection phase gratings. Journal of Physics D: Applied Physics 1999;32(4): 412–6.
[13] Furlani EP, Lee EH, Luo H. Analysis of grating light valves with partial surface electrodes. Journal of Applied Physics 1998;83(2):629–34.
[14] Gilbert JR, Ananthasuresh GK, Senturia SD. 3D modeling of contact problems and hysteresis in coupled electro-mechanics. Proceedings of the IEEE Micro Electro Mechanical Systems. 1996, p. 127–32.
[15] He Y, Marchetti J, Gallegos C. General contact and hysteresis analysis of multi-dielectric MEMS devices under thermal and electrostatic actuation. American Society of Mechanical Engineers, Dynamic Systems and Control Division (Publication); 1998, p. 323–8 DSC 66.
[16] Hinton E, Rock T, Zienkiewicz OC. A note on mass lumping and related processes in the finite element method. Earthquake Engineering and Structural Dynamics 1976;4:145–249.
[17] Hirota G, Fisher S, State A, Lee C, Fuchs H. An implicit finite element method for elastic solids in contact. 14th IEEE Conference on Computer Animation, Nov 7–8. 2001, p. 136–46.
[18] Horrigmoe G. Finite element instability of free-form shells. Ph.D. thesis, The University of Trondheim, Norway, Division of Structural Mechanics, the Norwegian Institute of Technology; 1977.
[19] Horrigmoe G. Hybrid stress finite element model for non-linear shell problems. International Journal for Numerical Methods in Engineering 1978;12:1819–39.
[20] Humar JL. Dynamics of structures. Series in Civil and Engineering Mechanics. Prentice Hall International; 1990.
[21] Keating DJ, Ho L. Effects of squeezed film damping on dynamic finite element analyses of MEMS. Proceedings of the SPIE 4408. 2001, p. 226–36.
[22] Kowarz MW. Spatial light modulator with conformal grating device. US Patent 6,307,663; 2001.
[23] Kowarz MW, Brazas JCJ, Phalen JG. Conformal grating electromechanical system (GEMS) for high-speed digital light modulation. IEEE 15th International Conference on Micro Electro Mechanical Systems Digest. 2002, p. 568–73.
[24] Kowarz MW, Lebens JA. Method for manufacturing a mechanical conformal grating device. US Patent Application Publication US 2001/0024325 Al; 2001.
[25] Kurzweg TP, Martinez JA, Levitan SP, Davare AJ, Kahrs M, Chiarulli DM. System simulation of a GLV projection system. MOEMS Display and Imaging Systems, vol. 4985. SPIE; 2003, p. 160–71.
[26] Lund JL, Wise KD. Chip-level encapsulation of implantable CMOS microelectrode arrays. Technical digest solid-state sensor and actuator workshop. 1994, p. 29–32.
[27] Meier RE. DMD pixel mechanics simulation. Texas Instruments Technical Journal 1998;15(3):64–74.

[28] Melosh RJ. A stiffness matrix for the analysis of thin plates in bending. Journal of Aeronautical Sciences 1961;38:34–42.
[29] Nabors K, White J. FastCap: a multipole accelerated 3-D capacitance extraction program. IEEE Transactions on Computer Aided Design 1991;10(11):1447–59.
[30] Nail T, Longmire EK, Mantell SC. Dynamic response of a cantilever in liquid near a solid wall. Sensors and Actuators, A: Physical, v 102, n 3. 2003, p. 240–54.
[31] Newmark NM. A method of computation for structural dynamics. American Society of Civil Engineers, Journal of Engineering Mechanics 1959;85(EM3):67–94.
[32] Oden JT. Calculation of geometric stiffness matrices for complex structures. AIAA Journal 1966;4(8):1480–2.
[33] Osterberg P, Yie H, Cai J, White J, Senturia S. Self-consistent simulation and modeling of electrostatically deformed diaphragms. Proceedings of the IEEE Micro Electro Mechanical Systems. 1994a, p. 28–32.
[34] Osterberg PM, Gupta RK, Gilbert JR, Senturia SD. Quantative models for the measurement of residual stress, Poisson ratio and Young's modulus using electrostatic pull-in of beams and diaphragms. Technical Digest Solid State Sensor and Actuator Workshop. 1994b, p. 184–8.
[35] Pian THH. Finite element methods by variational principles with relaxed continuity requirement. The mathematical foundations of the finite element method with application to partial differential equations. Academic Press, New York. 1973.
[36] Rajasekaran S, Murray DW. Incremental finite element matrices. Journal of the Structural Division 1973;99(12):2423–38.
[37] Senturia SD, Aluru N, White J. Simulating the behaviour of MEMS devices: computational methods and needs. IEEE Computational Science and Engineering 1997;4(1):30–43.
[38] Shames IH, Dym CL. Energy and Finite Element Methods in Structural Mechanics. Taylor & Francis; 1991.
[39] Solgaard O. Integrated Semiconductor Light Modulators for Fiber-Optic and Display Applications. Ph.D. thesis. Stanford (CA): Stanford University Electrical Engineering; 1992.
[40] Vemuri S, Fedder GK, Mukherjee T. Low-Order Squeeze Film Model for Simulation of MEMS Devices. Technical Proceedings of the MSM 2000 International Conference on Modeling and Simulation of Microsystems. 2000.